JOM, Vol. 71, No. 1, 2019
https://doi.org/10.1007/s11837-018-3156-x
© 2018 The Minerals, Metals & Materials Society

APPLICATION OF ATOMIC LAYER DEPOSITION FOR FUNCTIONAL NANOMATERIALS

UV-Ozone Functionalization of 2D Materials

STEPHEN J. MCDONNELL[1,3] and ROBERT M. WALLACE[2]

1.—Department of Materials Science and Engineering, University of Virginia, Charlottesville, VA 22904, USA. 2.—Department of Materials Science and Engineering, University of Texas at Dallas, Richardson, TX 75080, USA. 3.—e-mail: mcdonnell@virginia.edu

Integrating two-dimensional (2D) materials into the current nanoelectronic process requires control over the deposition of gate oxides onto these materials. Atomic layer deposition (ALD) relies on surface dangling bonds that are scarce for 2D materials. This review summarizes the advances made in understanding and controlling the nucleation of ALD oxides on these materials. As an example, we focus on ozone-based processes including UV-ozone pretreatments, which we have found to effectively functionalize the surface of molybdenum disulfide. Furthermore, we discuss the advantages and limitations of various functionalization or seeding techniques, such as limits in scalability or damage to the 2D materials.

INTRODUCTION

2D Materials

These first decades of the twenty-first century have seen a growing interest in 2D materials for nanoelectronic applications. The most recent renaissance was ignited with the isolation of (monolayer) graphene[1,2] from graphite through exfoliation inspired by prior work on graphite,[3,4] synthesis by a combination of chemical vapor deposition with carbon solubility behavior in metals such as copper,[5,6] as well as epitaxial growth on SiC.[7,8] Some of these materials, such as MoS_2, have been studied for almost a century due to their application as a dry lubricant.[9] In the latter half of the twentieth century, there was also considerable interest in their photoelectrochemical properties[10–12] and the photovoltaic effect in MoS_2 Schottky junctions[13] was also reported. However, despite sporadic reports on monolayer 2D materials including “a single carbon hexagonal layer”[14] and a “single-layer MoS_2,”[15] it was not until the seminal work of Novoselov and Geim[1,2] that the interest in monolayer 2D for nanoelectronics saw a dramatic rise. Similarly, it was following the 2011 demonstration of a monolayer MoS_2 transistor[16] that interest in graphene analogs, such as transition metal dichalcogenides (TMDCs), saw a similar rise in the number of publications per year. The total publications for MoS_2 per year as determined by Web of Science[17] are shown in Fig. 1. These proof-of-concept demonstrations of the potential for these materials motivated investigations into the integration of these materials into standard semiconductor processes.

With such 2D materials, which are dominated by sp^2 electronic hybridization, the surface chemistry (bonding) plays an important role in their properties, as well as in their integration in devices. For example, ideally such materials would exhibit a dearth of dangling bonds relative to typical 3D materials rendering them relatively chemically (and thus electrically) “inert” and thus interacting with other layers through van der Waals (VdW) forces.[18] The presence of surface defects, such as vacancies, as well as (step) edges would of course alter such 2D “surface” properties. Such defects would be naturally expected in the event of a “violent” exfoliation process where separation may not be confined to a single layer. Reviews of the history and progress for 2D materials, such as graphene,[19,20] boron-nitride,[21,22] and TMDCs,[9,23,24] have been offered for interested researchers.

Atomic Layer Deposition

Atomic layer deposition (ALD) is now a standard industry tool for the deposition of ultra-thin films, and the mechanisms have been covered in a review by S. George.[25] Briefly, ALD works by sequentially exposing a surface to precursor species that can react with the surface to form self-limiting monolayers, which is shown schematically in Fig. 2.[26] In

(Published online October 4, 2018)

reality the layer is typically less than one monolayer due to steric hindrance effects. In the ALD process regime, the layer cannot become greater than one monolayer because the precursor will not react with itself. After purging the first precursor gas from the system, a second precursor is introduced that can react with the first precursor but not with itself. By alternating precursor 1 and 2 pulses, interrupted with purging steps, the deposition can then be controlled with atomic layer precision. Two aspects are critical to ALD: (1) The precursors must be separated by a purge to avoid conventional CVD growth that would result in greater than one monolayer per cycle growth; and (2) the precursor must be able to react with the substrate to nucleate. So this leads us to the following question: How do we to nucleate precursors on a surface with a low density of dangling bonds associated with 2D materials?[27,28]

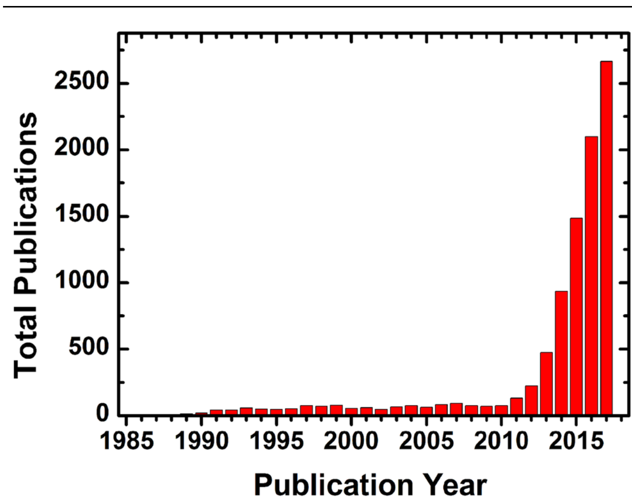

Fig. 1. Total number of publications on the topic of "MoS_2" from 1985 to 2018. Data are taken from a Web of Science search refined to include only the disciplines of materials science multi-disciplinary, applied physics, nanoscience nanotechnology, and electrochemistry.

Nucleating on Inert Surfaces

The problem with nucleating ALD on inert surfaces may be illustrated in prior work with carbon nanotubes.[29] Farmer and Gordon found that the metal precursor did not actually covalently bond to the CNT, and that deposition was only possible when the oxidizing precursor (e.g., NO_2) was added after only a short purge time (7 s). The authors concluded that this enabled the oxidizing species to react with the metal precursors that were only physisorbed to the surface and thus prevent desorption. This process was referred to as "non-covalent functionalization." Such methods were subsequently also extended to enable graphene-based devices.[30]

Ozone (O_3) is a more common oxidation precursor in ALD processes and has been widely adopted in the semiconductor industry.[31] Moreover, the utilization of O_3 for surface cleaning and preparation processes, as well as ultrathin oxide formation in the semiconductor industry, is well established.[32–38] Given such process adoptions, an alternative approach using O_3 for the functionalization of

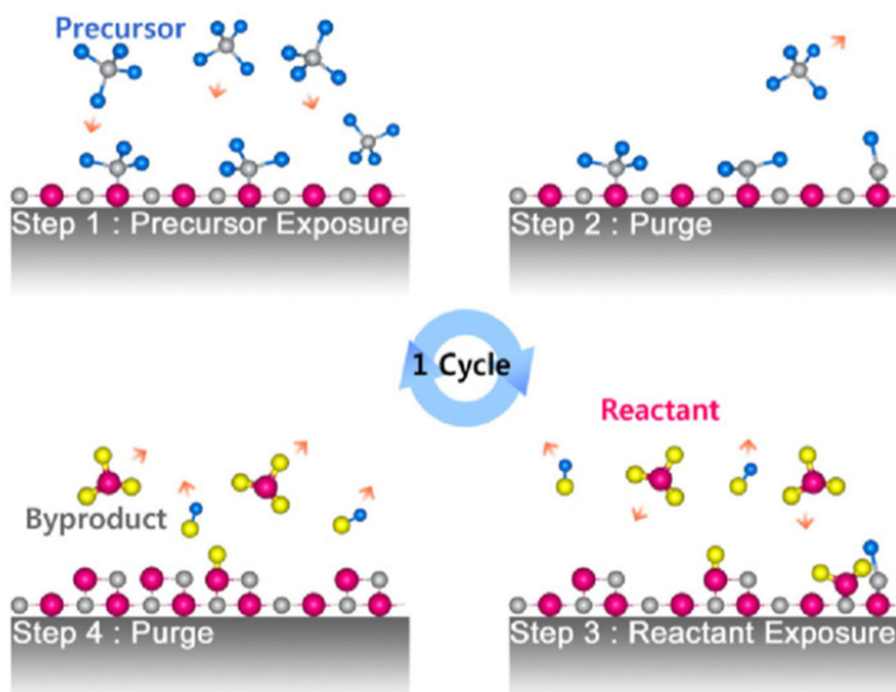

Fig. 2. Schematic of the TMA + H_2O ALD process for depositing Al_2O_3. Reprinted from Thin Solid Films, 517/8, H. Kim et al., *Applications of atomic layer deposition to nanofabrication and emerging nanodevices*, pp. 2563–2580. Copyright (2009), with permission from Elsevier.

graphite surfaces[39–42] and graphene[43] for subsequent ALD growth was also examined.

The production of O_3 can be accomplished through a photochemical process with O_2 and ultraviolet light in the vicinity of the surface,[32,33] as well as in remotely generated sources. Thus, reactive species such as atomic O and O_3 are available at low temperatures (e.g., 300 K) for surface chemical reactions from such processes. It has been found that, in the case of graphene, that the utilization of a UV-O_3 source can generate defects in graphene through C-C bond scission (i.e., etching), while remotely generated O_3 results in a somewhat less defect concentration.[42,44] Therefore, care must be made in the choice of the O_3 production method and the effect on the graphene surface where etching can be catastrophic.

Early work on graphene integration used highly oriented pyrolytic graphite as a substitute for graphene flakes to probe surface and interface chemistry with large area analytical techniques. It was found that the ALD process resulted in growth only on the step edges of graphite surfaces, as shown in Fig. 3. It was also shown that surface pretreatments with ozone could improve the uniformity of subsequent ALD thin films.[39,40]

For the ideal graphite/graphene surface, theoretical modeling suggests that remotely generated O_3 may generate a weakly bound surface epoxide species that serves as an initial functionalization route in the ALD process for Al_2O_3 growth on graphite/graphene.[45] Such species may be detected in surface analysis techniques such as x-ray photoelectron spectroscopy (XPS).[39] Theoretical predictions suggest that epoxide species formation is easily reversible, and thus, it avoids etching of the underlying carbon layer enabling a VdW-coupled dielectric layer on graphene.

In addition to the O_3 surface functionalization mechanism, surface contamination could also play a role in ALD nucleation on the graphite/graphene surface. This is particularly important when device fabrication uses polymers and solvents that, at the atomic level, may leave chemical residues in place without further cleaning treatments.[46,47] Additionally, physisorbed species from atmospheric exposure of the exfoliated surface may be present that may enhance nucleation, and in the ALD process sequence, annealing may impact the subsequent deposition uniformity.[41]

A detailed in situ XPS study of the factors involved for functionalization by remotely generated O_3 and subsequent Al_2O_3 ALD on graphite was performed by McDonnell et al.[42] Exposure of exfoliated surface to $< 1 \times 10^8$ L of O_3 [1 Langmuir (L) $\equiv$ 1×10^{-6} Torr s] at room temperature was found to primarily impact surface contamination, while higher doses result in clear, detectable interactions with the graphite surface, which are more likely hydroxyl species rather than epoxides. A comparison of the precursor exposure order (viz. metal "first" versus O_3 "first") in the ALD process at room temperature revealed that O_3 surface cleaning of contaminants plays an important role in the Al_2O_3 growth, with step edge nucleation dominant in the O_3-first process. Such behavior is attributed to relatively poor growth in the basal plane regions cleaned by the O_3-first exposure. In contrast, the metal-first precursor exposure results in a more conformal film growth, likely nucleated by the underlying surface contamination.

The impact of the N_2 purge time between precursor pulses on the interfacial chemicals states was also studied showing that concentration of partial reaction products is dependent on the purge time. Moreover, depending on the ALD deposition temperature, metal precursor partial reaction products from the associated ligand decomposition could be detected. It was found that longer purge times tended to decrease the partial reaction product concentration pointing to the importance of the precursor residence time on the surface relative to the purge time.

Such studies on a "monoelemental" 2D surface provide insight for the sort of ALD reactions that occur on 2D compounds, such as dichalcogenides, which are presented in the next section.

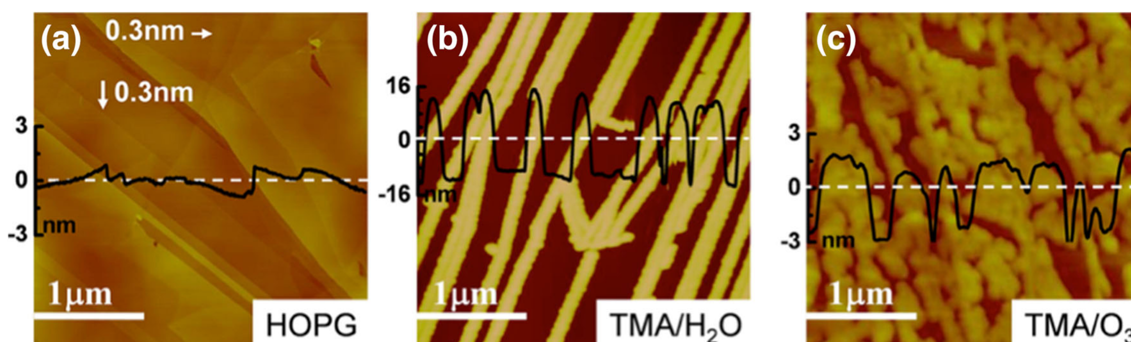

Fig. 3. (a) AFM image of fresh HOPG surface and (b) the sample with Al_2O_3 layer deposited from TMA/H_2O (200 cycles) process (c) with Al_2O_3 layer from TMA/O_3 process (50 cycles). Reprinted with permission from Lee et al., *Appl. Phys. Lett.* 92, 203,102 (2008) AIP Publishing.

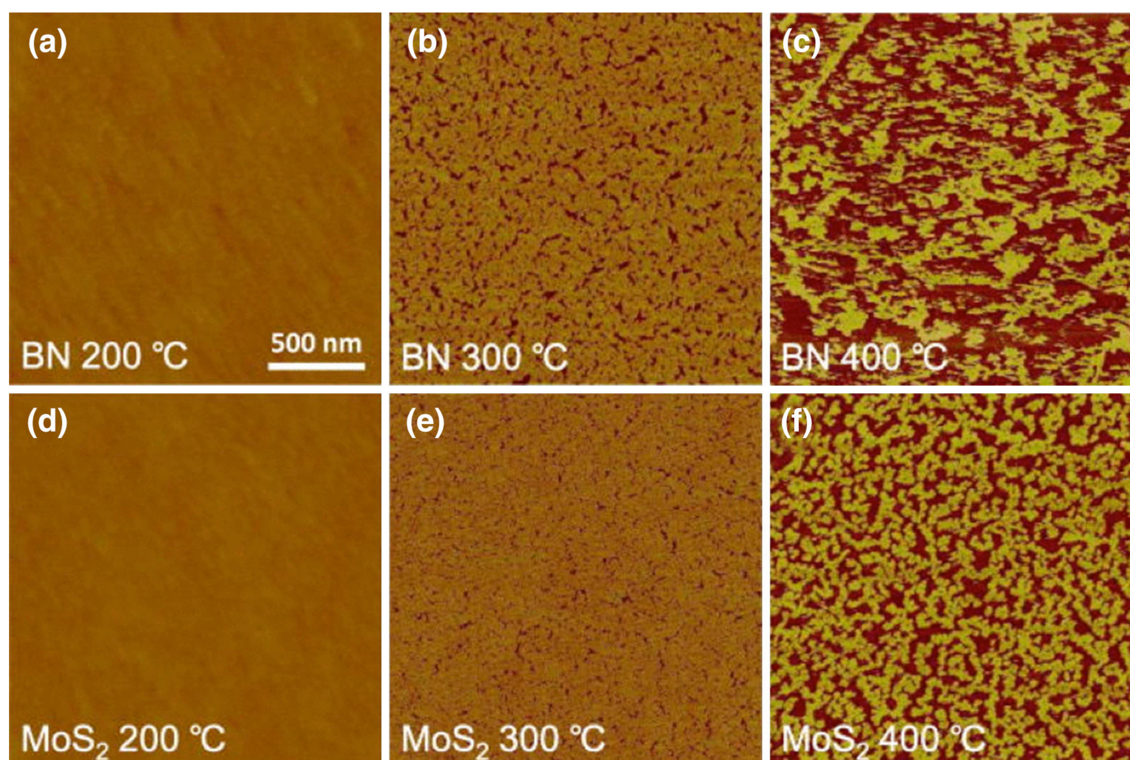

Fig. 4. AFM images of BN (a–c) and MoS_2 (d–f) surface after 111 cycles of ALD Al_2O_3 at 200°C (a and d), 300°C (b and e), and 400°C (c and f). All images are taken in a 2-μm by 2-μm region with a scale bar of 500 nm. Reprinted with permission from Liu et al., *Appl. Phys. Lett.* 100, 152,115 (2012) AIP Publishing.

ALD on TMDCs

Given the known issues with nucleating ALD on graphite, it was therefore somewhat surprising to find that the early reports of MoS_2 and WSe_2 based transistors used ALD gate oxides without reporting any deliberate functionalization of the surface.[16,48–50] An early explanation for this discrepancy was offered by Liu et al. who reported temperature-dependent uniformity for Al_2O_3 thin films on MoS_2 and BN, as shown in Fig. 4.[51] Using a Lennard-Jones potential model, the authors suggested that precursor-substrate interactions are stronger for precursor-MoS_2 and precursor-BN than they are for precursor-graphene. While this appeared to be a satisfactory explanation, the authors had employed a 6-s purge during their ALD process, which was very similar to the early non-covalent functionalization process used by Farmer and Gordon when studying ALD on carbon nanotubes.[29] Furthermore, in all of the preceding reports of uniform ALD on TMDCs, the samples had been "processed" for device fabrication, which included exposure to combinations of adhesives, solvents, and polymers (e.g., photoresists). It is therefore likely that surface contaminates or modified ALD processes confounded these results by playing an active role in precursor nucleation.

Precursor Nucleation on TMDCs

In an attempt to better understand the intrinsic nucleation of ALD precursors on TMDCs, in vacuo ALD-XPS was again employed to study the ALD of high-κ dielectrics on MoS_2. In contrast to the prior reports of uniform gate oxide depositions on TMDCs, we found that both HfO_2 and Al_2O_3 were highly non-conformal, as shown in Fig. 5.[52,53] McDonnell et al. also showed that exposures to polymers and/or solvents could dramatically influence the nucleation of HfO_2 on MoS_2. This confirmed that process residues may well have also played a role in enabling uniform ALD growth of gate oxides on TMDCs in the original reports of TMDC based transistors.

The initial precursor adsorption was also investigated by employing a "half-cycle" ALD deposition-characterization process.[52] This experiment involves exposing a surface to only one precursor (e.g., metal) and subsequently probing the surface chemistry with XPS before returning the sample to the ALD reactor for exposure to the second precursor (e.g., oxidant). The entire experiment took place in a coupled ALD-UHV deposition and characterization tool described elsewhere.[54] This process inherently simulated extremely long purge times since the sample would be in UHV for 2–3 h

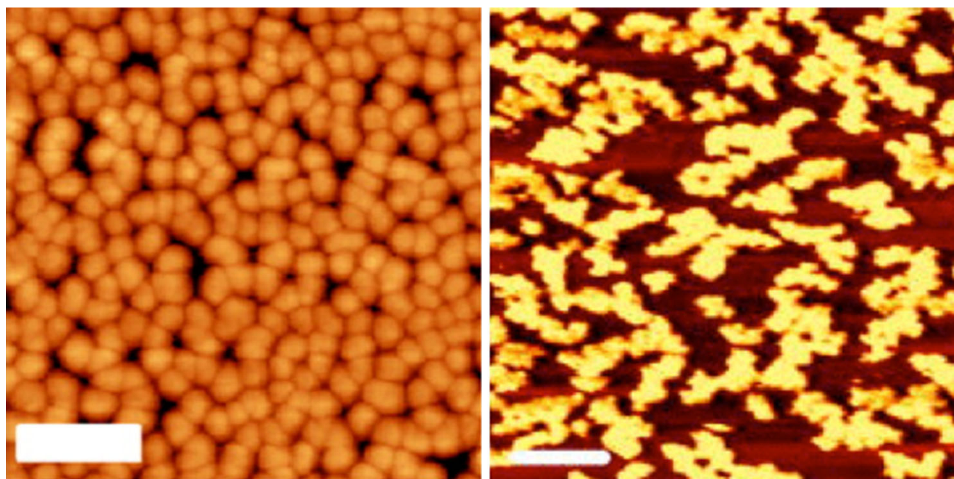

Fig. 5. AFM images of (left panel) 150 cycles of ALD HfO_2 on MoS_2 100-nm scale bar, and (Right panel) 30 cycles of Al_2O_3 on MoS_2 scale bar 200 nm. Reprinted (adapted) with permission from McDonnell et al., *ACS Nano*, 2013, *7* (11), pp 10,354–10,361. Copyright (2013) American Chemical Society, and Azcatl et al., *Appl. Phys. Lett.* 104, 111,601 (2014) with the permission of AIP Publishing.

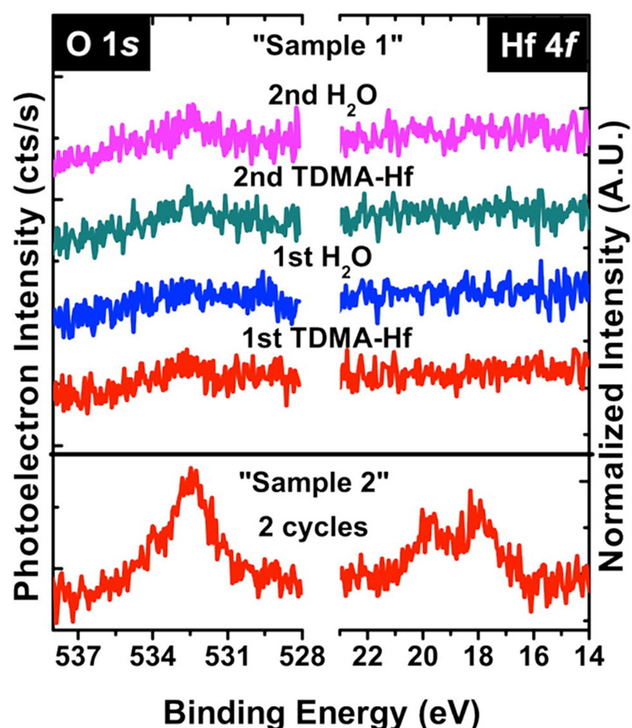

Fig. 6. XPS core-level spectra of the O 1*s* and Hf 4*f* regions for two full cycles of TDMA-Hf, H_2O, H_2O deposited by (Top) half-cycle and (bottom) uninterrupted depositions. Reprinted with permission from McDonnell et al., *ACS Nano*, 2013, *7* (11), pp. 10,354–10,361. Copyright (2013) American Chemical Society.

between precursor pulses to acquire XPS data. It should be noted that these experiments were highly successful in studying the initial precursor nucleation of III-V semiconductor substrates since even partial monolayer coverage of a metal precursor is readily detected with XPS.[55]

In the study of HfO_2 ALD on MoS_2, the authors began by exposing a geological MoS_2 crystal (clean by mechanical exfoliated) to the tetrakis (dimethylamino) hafnium (TDMA-Hf) precursor at a substrate temperature of 200°C for 0.1 s. This exposure was modeled on an earlier report of HfO_2/MoS_2 transistors that used TDMA-Hf precursors to deposit uniform HfO_2. The results of this half-cycle experiment are shown in the upper section of Fig. 6. It is clear that after 2 full cycles (4 half-cycle steps), there was no HfO_2 detected on the surface. This could have suggested an incubation period for deposition. However, using a fresh sample and carrying out 2 full cycles, with no UHV breaks to acquire XPS, yielded the markedly different results shown in the lower section of Fig. 6. It is clear that when the deposition process is not broken up to allow for characterization, some nucleation can occur. The details of each full cycle were TDMA (0.1 s) + N_2 purge (5 s) + H_2O (0.1 s) + N_2 purge (10 s) + H_2O (0.1 s) + N_2 purge (10 s) after Radisavljevic et al.[16] Again, we note that the purge after the metal precursor was only 5 s, which is similar to the 6 s employed by Lie et al.[51] and the 7 s suggested for non-covalent functionalization[29] of carbon nanotube.

This short purge-time-enabled nucleation was explained by considering both a qualitative Lennard-Jones potential model, as well as the details of the purge efficiencies reported by Hausmann.[56] Hausmann studied the influence of purge time on the deposition rate of HfO_2 and ZrO_2 on SiO_2/Si substrates. Noting that true ALD has a self-limiting thickness per cycle that cannot be exceeded by increasing precursor exposure times, it was shown that decreasing the purge time resulted in increasing deposition rates beyond this limit. This is explained by the simultaneous residence of both physisorbed precursors on the surface. For example, once the surface is saturated with reacted metal precursor molecules, no more can attach to the surface. However, some may physisorb temporarily. Prior to exposing the sample to the oxidizing

precursor, a sufficiently long purge ensures not only that all gaseous metal precursors are removed from the chamber, but also that all physisorbed precursors have desorbed from the sample surface. If the purge time is sufficiently short such that the gaseous species are removed but some physisorbed species remain on the surface, then the subsequent oxidation precursor can react with both the self-limiting reacted metal precursor layer and the physisorbed precursor that remains on the surface. This leads to a deposition rate greater than expected.

When this reasoning is applied to the HfO_2 deposition on MoS_2, we can explain the differing results for half-cycle and uninterrupted cycle depositions shown in Fig. 6. Following the initial metal precursor pulse, the surface is saturated with the TDMA-Hf molecules. Unlike the model case of TMA-silicon, the TDMA-Hf does not dissociate on the surface due to the lack of reactive cites. Therefore, during the subsequent purging step that removes the gaseous TDMA-Hf from the chamber, the physisorbed TDMA-Hf molecules will also be removed. However, this removal is not instantaneous, so by employing sufficiently short purge times, some of the physisorbed species will still reside on the surface during the oxidation pulse, resulting in the formation of an oxidized metal molecule that was speculated to be less volatile than the TDMA-HF precursor, therefore, allowing it to remain on the surface. So, when the sample is exposed to UHV for 2–3 h, there is ample time for the precursors to desorb. In fact, since no metal precursors are detected by XPS, we assume that this desorption occurs within the minutes required to transfer the sample between coupled chambers. This leads to no detectable deposition. However, when the purge time of 5 s is employed, the subsequent reaction of the H_2O with the mobile TMDA-Hf precursors on the surface leads to deposition. Furthermore, evidence for the absence of a “true” ALD of HfO_2 on MoS_2 is found in the deposition rate reported by Radisavljevic, which was 0.19 nm/cycle.[16] This is more than double the self-limiting deposition rate of 0.09 nm/cycle that is typically reported for TDMA-Hf on more reactive SiO_2 and III-V substrates.[56,57] This strongly suggests that such a process lies outside of the ALD regime.

It was noted that the short precursor time alone was not sufficient to result in uniform deposition. After 150 ALD cycles, the resultant HfO_2 was in 15-nm islands with the bare MoS_2 exposed beneath as demonstrated using low-energy ion scattering spectroscopy. These results are summarized in Fig. 7. Instead it was shown that solvents and polymer residues could enhance nucleation and likely aided the deposition of pin-hole, free high-κ dielectrics on

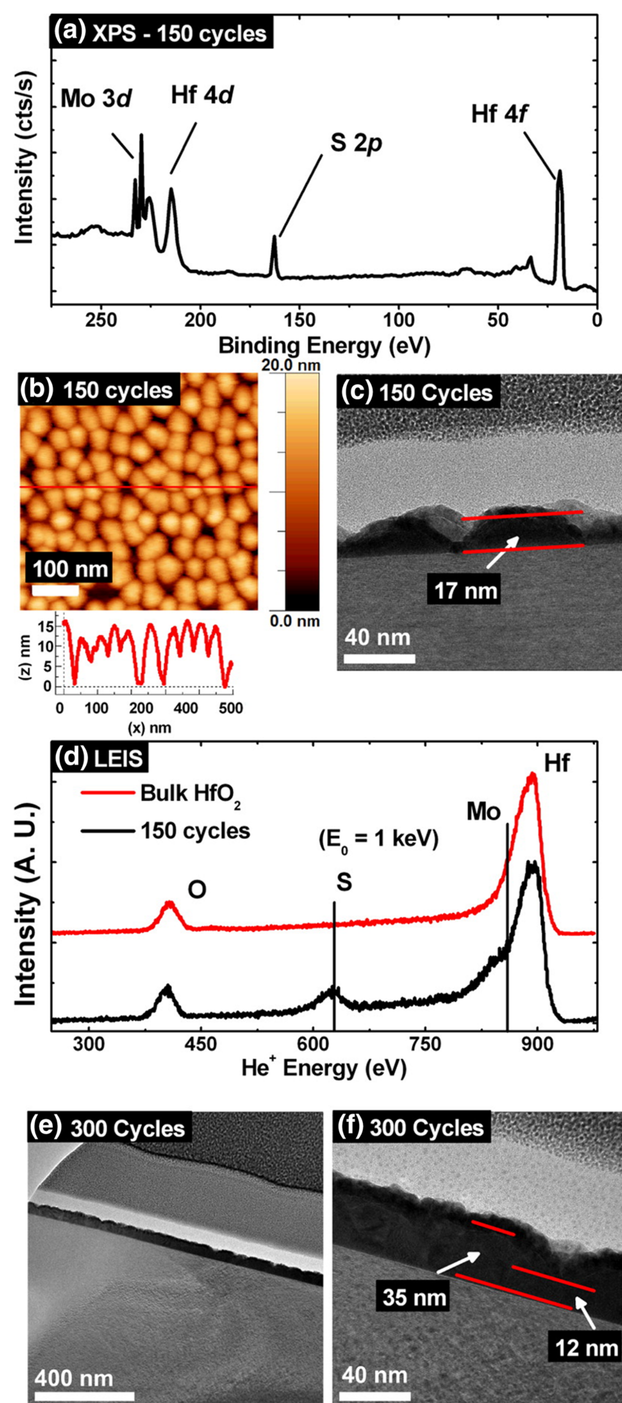

Fig. 7. (a) XPS for HfO_2/MoS_2 stack after 150 cycles of ALD (b) 0.5 $\times$ 0.5-μm AFM image of the same HfO_2/MoS_2 stack (c) transmission electron microscopy (TEM) images of a $Pt/SiO_2/Pd/HfO_2/MoS_2$ stack with 150 cycles of HfO_2 ALD on MOS_2 (40-nm scale bar). (d) LEIS spectra taken after 150 cycles (black, bottom) and bulk HfO_2 on Si (red, top). (e) TEM image of a $Pt/SiO_2/Pd/HfO_2/MoS_2$ stack with 300 cycles of HfO_2 ALD on MoS_2 (400-nm scale bar). (f) TEM image of a $Pt/SiO_2/Pd/HfO_2/MoS_2$ stack with 300 cycles of HfO_2 ALD on MoS_2 (40-nm scale bar). Reprinted with permission from McDonnell et al., *ACS Nano*, 2013, *7* (11), pp. 10,354–10,361. Copyright (2013) American Chemical Society (Color figure online).

MoS_2 and WSe_2.[52] A recent report by Lin et al. deliberately used these short purge times in conjunction with low deposition temperatures (80°C) to enhance the nucleation of Al_2O_3 on MoS_2.[58] We also note that in the purge time dependence study by Hausmann et al., they reported on the role of flow rate and temperature.[56] Therefore the specifics of an ALD reactor are important when determining the length of the purge that would be sufficient to promote or avoid this unreacted precursor–precursor interaction regime. For example, Zou et al. demonstrated uniform ALD of HfO_2 on MoS_2. In that work, the authors used 120-s and 100-s purges after the metal (TDMA-Hf) and water precursor but the substrate temperature was only 95°C.[59] This lower substrate temperature increases the residence time of physisorbed precursors and enables deposition. It was noted that the deposition rate in this case was 0.14 nm/cycle, which again exceeded that of the true ALD regime.

The preceding discussion has focused on the TDMA-Hf precursor, which is the most commonly reported precursor of ALD HfO_2 on MoS_2. In a first principles study of the $HfCl_4$, HfI_4, TEMA-Hf, and TDMA-Hf precursor interactions with OH terminated surfaces, the authors supported the use of TDMA-Hf due to the corrosive by-products resulting from $HfCl_4$ and HfI_4 as well as the higher activation energy of the TEMA-Hf ethyl group compared to TDMA-Hf.[60] A detailed comparison of how the precursor type influences the nucleation on 2D materials may yield useful insight.

Functionalization

The unintentional (and thus uncontrolled) functionalization of 2D surfaces is not likely a viable, reproducible integration solution for nucleating ALD on MoS_2. While there continue to be reports of device structures fabricated with the method,[59,61] variations in photoresist and cleaning methods will likely leave different residues resulting in variations in uniformity, and more importantly interface quality, from process to process. It is therefore important to develop a repeatable and scalable functionalization process for 2D materials. Moreover, in the limit of a monolayer or few layer materials, any perturbation of electronic structure of the topmost layer is likely to be unacceptable. This provides us with clear criteria for a functionalization process: repeatable, scalable, and no perturbation of electronic structure.

A number of processes have been proposed and studied with the goal of achieving this. One of the most common is to simply nucleate the ALD by first depositing a seed layer. This is often a thin metal or metal oxide layer by physical vapor deposition. This works well because physical vapor deposition does not rely on a surface dangle bond to the same extent as a chemical vapor process such as ALD. Examples of seed layers on 2D materials have been SiO_x,[62] Yttria,[63] aluminum,[64–66] and titianium.[67] It was later shown that such a process is not scalable to ultra-thin dielectrics on CVD graphene since process residues lead to clustering of the metal seed layer.[68] Furthermore, metals such as Ti are known to react with MoS_2 and other TMDCs making such a seed layer inappropriate for TMDCs.[69–72] The use of Al or other metals is likely to be limited by process residues, as was the case for graphene. Another seeding strategy is the use of self-assembled molecules such as PTCDA or Phthalocyanine.[73,74] Plasma oxidation of the MoS_2 surface has also been employed and resulted in highly conformal Al_2O_3 films; however, XPS characterization showed the presence of oxidized Mo at the interface suggesting the plasma process resulted in Mo-S bond scission.[75] Interestingly, while it was not discussed by the authors, the Mo 3*d* core-level spectra showed evidence of potential metallic Mo in addition to Mo-S and Mo-O bonds following the plasma treatment.

UV-Ozone

As previously discussed, UV-Ozone has been used to clean organic contamination from surfaces.[32,33,76] In the work of Azcatl et al., an MoS_2 crystal was exposed to UV-Ozone.[53] This was achieved in a UHV chamber filled with a partial pressure of

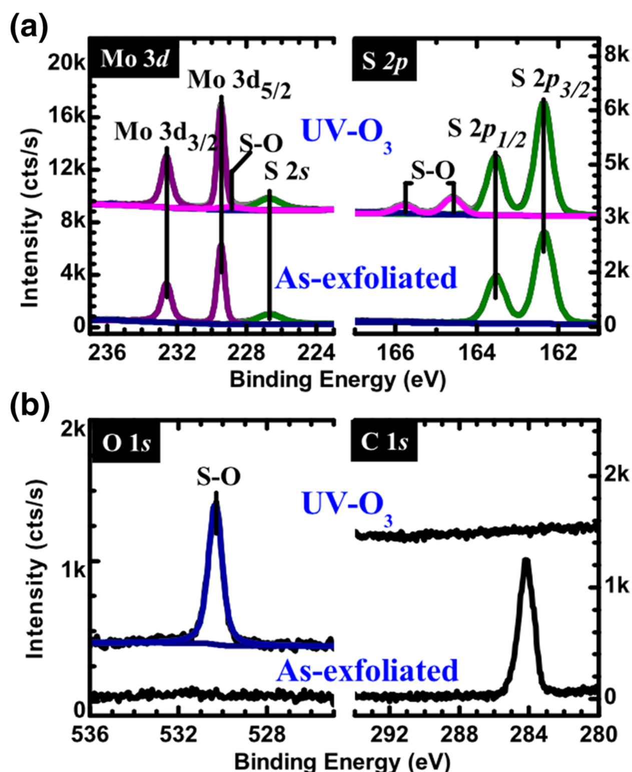

Fig. 8. XPS of MoS_2 before and after UV-ozone treatment. (a) shows no change in the Mo 3d core-level line shape, while evidence of new Mo-S-O bonds are seen in the S 2p core-level. (b) shows the concurrent increase in the O 1-s signal and the expected removal organic species. Reprinted from Azcatl et al., *Appl. Phys. Lett.* 104, 111,601 (2014) with the permission of AIP Publishing.

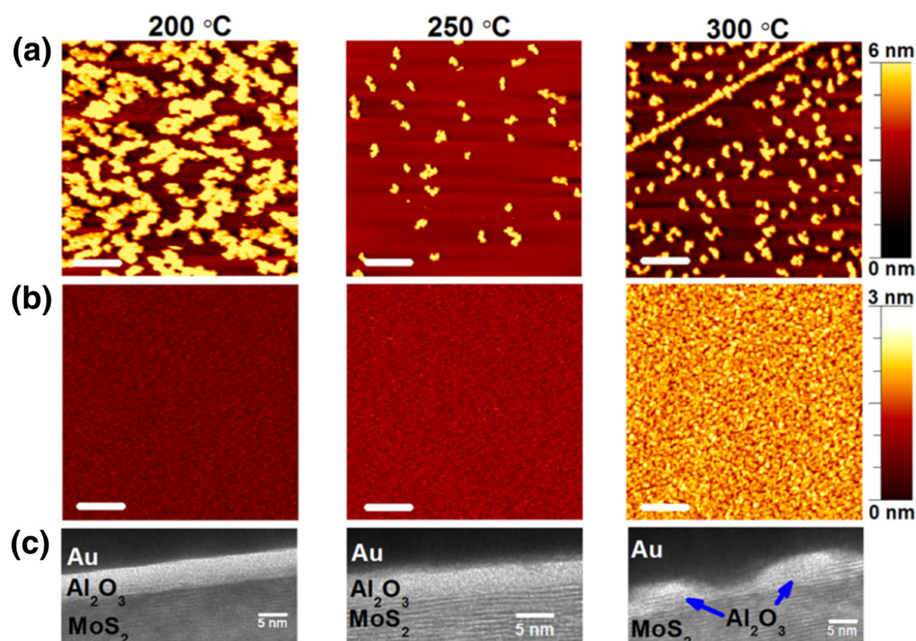

Fig. 9. Atomic force microscopy images of Al_2O_3 deposited by 30 ALD cycles at 200°C, 250°C, and 300°C on (a) as exfoliated bulk MoS_2 and (b) oxygen functionalized MoS_2 (O-S-MoS). Scale bar: 200 nm. (c) HRTEM images of the corresponding films shown in (b). Reprinted from Azcatl et al., *Appl. Phys. Lett.* 104, 111,601 (2014) with the permission of AIP Publishing.

900 mbar while the sample was held within a few millimeters for a low-pressure mercury lamp. As expected, the organic surface contamination was removed by this process as evidenced by the elimination of the C 1s core-level observed from in vacuo XPS, as well as the sharpening of the diffraction spots in low-energy electron diffraction. As shown in Fig. 8, the authors also observed a new sulfur state via XPS analysis. The binding energy of the new state, which was 164.8 eV, does not correspond to known sulfur oxides. Furthermore, no new chemical states were observed in the Mo 3d core level, which suggested that no Mo-S bond scission had occurred within the XPS detection limit. This result is markedly different from the oxidized and potentially metallic features observed in the Mo 3d core level after oxygen plasma treatments.[75] The new sulfur feature at 164.8 eV was explained as a rehybridization of the topmost sulfur atoms to bond with oxygen without breaking their sulfur-molybdenum bonds (O-S-MoS). This was supported by first principles calculations, which suggested that a single oxygen atom adsorbed on the surface of MoS_2 has a formation energy of –0.81 eV.

Importantly, this adsorbed oxygen was found to serve as a nucleation layer for subsequent ALD (TMA and H_2O precursors). Figure 9 shows AFM and TEM images of Al_2O_3 thin films deposited by ALD in vacuo, on both bare and UV-ozone functionalized MoS_2 crystals. It is clear at all three deposition temperatures (200°C, 250°C, and 300°C), the UV-ozone treated surface results in enhanced nucleation. However, at 300°C, the films are not uniform. Also, at 250°C, the TEM images show some contrast variations in the Al_2O_3 indicating that the some uniformity or density variation may exist. However, the UV-ozone clearly enabled uniform ALD at a substrate temperature of 200°C. The authors explained this temperature-dependent uniformity by analyzing the functionalized MoS_2 as a function of temperature with no ALD deposition carried out. It was found that the adsorbed oxygen appears to desorb upon heating treatments. At 200°C, there remains detectable levels of O-S-MoS; this is on the limit of detection after a 250°C anneal and below the limit of detection after a 300°C anneal. This would seem to explain the temperature dependent uniformity since the stability of the functionalization layer is also temperature dependent.

Finally, the authors also showed that upon deposition of Al_2O_3 all evidence of the O-S-MoS bonding was below the limit of detection, even at 200°C. This was interpreted as being due to the incorporation of the weakly bonded oxygen into the Al_2O_3 dielectric. It was also shown from first principles that the adsorbed oxygen would not add states into the bandgap of MoS_2. Therefore, any remaining O-S-MoS bonds that could be below the limit of detection for XPS would not be expected to have a detrimental impact on the properties of the MoS_2.

Device Characterization of UV-Ozone Functionalized MoS_2

From a device perspective, the dielectric layer formed on semiconducting TMDC surfaces using O_3-functionalization routes must demonstrate

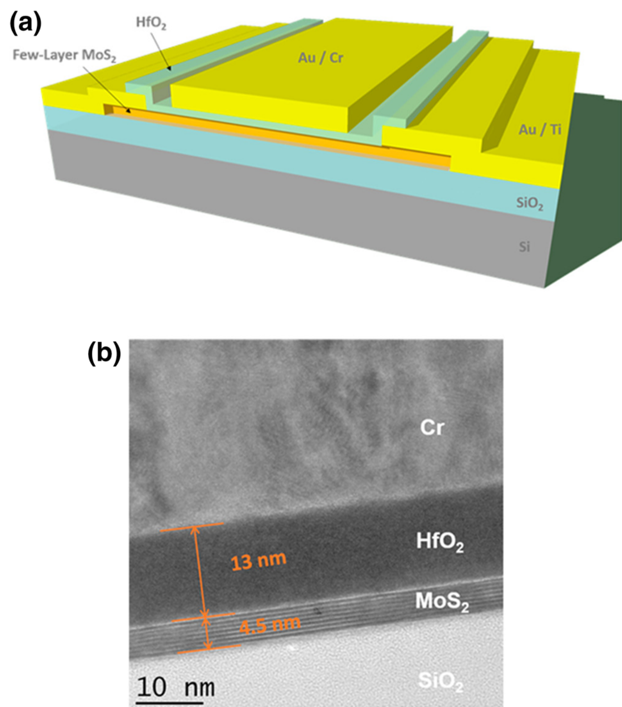

Fig. 10. (a) Schematic cross section of the top-gated MoS_2 field effect transistor structure. Gate stack: Au/Cr/HfO_2/MoS_2. (b) Cross-sectional transmission electron microscopic image of the metal/HfO_2/MoS_2 transistor gate stack. A 13-nm HfO_2 is uniformly deposited on a 7-layer MoS_2 flake. Reprinted with permission from Zhao et al., *ACS Appl. Mat. Interf.* 9 (28), 24,348 Copyright (2017) American Chemical Society.

useful properties. This has been recently examined for various gate electrode configurations (top and back) for MoS_2.[77–85]

By exploiting the O_3 surface functionalization approach for high-κ dielectric ALD, Zhao et al. demonstrated the ability to employ electrical characterization test structures incorporating a more conventional top gate geometry, thereby enabling an inroad to understanding the impact of defects at the high-κ/MoS_2 interface as well as those associated with the high-κ itself through impedance spectroscopy.[77,80,84]

Figure 10 presents the transistor test structure schematic and the associated TEM cross section of a top gate device stack achieved after HfO_2 ALD enabled by O_3-functionalization. It is seen that the physical characterization reveals a uniform HfO_2 deposition on the 7-layer exfoliated and transferred MoS_2 layer on SiO_2. Additionally, no unintentional oxidation (etching) of the MoS_2 is detected. The associated electrical characterization of the device structure is presented in Fig. 11.

It is seen (Fig. 11a) that the expected gate (leakage) current is minimized with the ALD HfO_2 gate dielectric, whereas an on/off drain current of 10^6 is readily observed, while the impact of the Schottky junctions is evident (Fig. 11b), and the capacitance–voltage characterization (Fig. 11c) reveals a significant defect response. It is noted in this work that the device fabrication process was not optimized (e.g., through appropriate post-deposition annealing) as the purpose was to establish the sensitivity of impedance measurements for such TMDC devices. Significant interfacial defects as well as defects in the high-κ dielectric (T_{ALD} = 200°C) are very much expected. The impact of annealing in N_2 and forming gas (N_2:H_2) has also been studied to better optimize the device response,[82] as well as the detailed extraction methods for interface defect traps and nearby (border) defect traps in the HfO_2 using these structures.[84]

The details of the device test structure and the electrical characterization and property extraction (e.g., D_{it}) remain a contemporary research topic in the community. Interface state density for HfO_2/MoS_2/SiO_2/Si on the order of 10^{13}/cm^2 eV as well as the presence of significant border traps in the high-κ dielectric has been reported.[80,84] Recent work demonstrated the impact of the choice of the *back-gate dielectric* (Al_2O_3 versus HfO_2) on the extracted D_{it} ($\sim 10^{11}$/cm^2 eV), the concomitant improvement in the measured sub-threshold slope ($\sim$ 69 mV/dec for Al_2O_3), and mobility of the associated transistors ($\sim$ 145 cm^2/Vs).[81,83,85] Preliminary studies on the impact of 400°C forming gas anneals on HfO_2/MoS_2 transistors showed a decrease in the threshold voltage, decrease in leakage current, and minimized I–V hysteresis.[82] The same study reported a slight increase in drive current and suggested this may be attributed to a degradation in contacts or the MoS_2 flake. Taken together, such work to date demonstrates promising, manufacturable avenues to control the electrically active defect population to produce a viable device technology on single crystal TMD grains (flakes). However, much work remains to be done on devices fabricated with large area, polycrystalline and high-quality (crystalline) TMD films as well.

Further work exploiting alternative back gate ALD dielectrics (instead of SiO_2) with such top gate transistor structures has also been recently reported enabling devices with substantially improved characteristics.[81,83,85] Subthreshold slopes of the drain current at the theoretical thermionic limit (60 mV/decade) have been reported. Taken together, the device results confirm that the O_3-functionalization process for high-κ ALD is quite useful for MoS_2 devices.

UV-Ozone Interactions with TMDCs

In a subsequent report by Azcatl et al. it was shown that the functionalization of MoS_2 worked equally well for HfO_2 deposited by ALD (TDMA-Hf and H_2O precursors).[86] Interestingly, the same process applied to $MoSe_2$ and WSe_2 crystals yielded some different results. In both cases both Se and Mo/W oxides were detected which suggests a more aggressive O_3 reaction with this substrate that led to bond scission. The authors monitored the progression of the interface chemistry as a function of

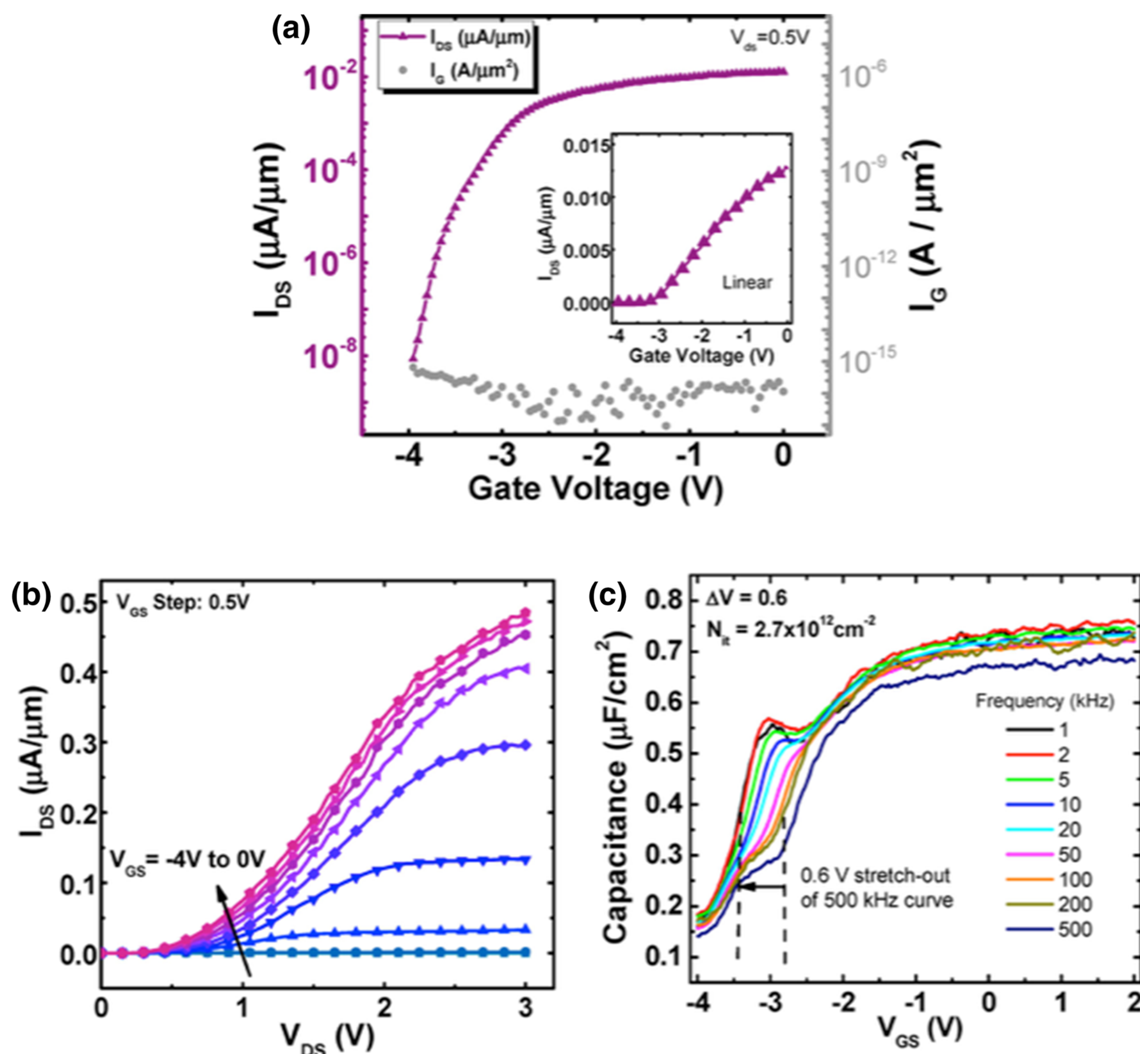

Fig. 11. Electrical characterization of device with 13 nm HfO_2 and 7-layer MoS_2 (L = 6.5 μm, W = 9.5 μm). (a) I_{DS}–V_{GS}: $I_{ON}/I_{OFF} = 10^6$ with ultralow gate leakage (b) I_{DS}–V_{DS} with V_{GS} from −4 to 0 V (c) C–V: frequency dependence, where a "hump" in the range −2.5 to −3.5 V indicates an interface defect response. The 0.6 V stretch-out of 500 kHz curve indicates the Fermi energy pinning at the MoS_2/HfO_2 interface. Reprinted with permission from Zhao et al., *ACS Appl. Mat. Interf.* 9 (28), 24,348 Copyright (2017) American Chemical Society.

sequential HfO_2 ALD depositions. Since molybdenum oxides are volatile and moderate temperatures, the subsequent deposition of HfO_2 led to a rapid decrease in Mo-O species and finally resulted in a sharp interface free of Mo-O or Se-O bonds with uniform HfO_2 coverage. However, for the Wse_2, while both the W-O and Se-O bonds were seen to reduce with each ALD cycle detectable W-O was still present even after 30 ALD cycles (~ 30 nm of HfO_2). Furthermore, a combination of TEM and AFM revealed evidence of Wse_2 etching and the final surface exhibited triangular islands. The high-resolution TEM images showing the lack of uniform coverage on WSe_2 is shown in Fig. 12.

While the work of Azcatl et al. showed O adsorption without Mo-S bond scission for UV-ozone treated MoS_2, other results can be found in the literature. Using back gated, few layer MoS_2, Guo et al. reported that exposing the MoS_2 to UV-O_3 yielded an increase in mobility of one order of magnitude.[87] The authors speculated that this was due to trap passivation by the photogenerated excess carriers during UV-O_3 plasma treatment. Interestingly the authors stated that Raman analysis was consistent with the presence of the thin Mo oxide layer, and they also confirmed that UV treatment alone (no ozone) did not yield a mobility enhancement. Recently, Su et al. replicated the process of Azcatl et al. on monolayer and multilayer MoS_2 flakes.[88] Their photoluminescence study revealed that the PL in monolayer MoS_2 was quenched and this was attributed to the adsorption of oxygen on the surface. Furthermore bilayer MoS_2 began to behave like monolayer MoS_2, i.e., the PL was enhanced. This PL enhancement was non-uniform and was attributed to the non-uniform adsorption on the surface. The authors noticed no etch pits on the flakes and so it possible that the

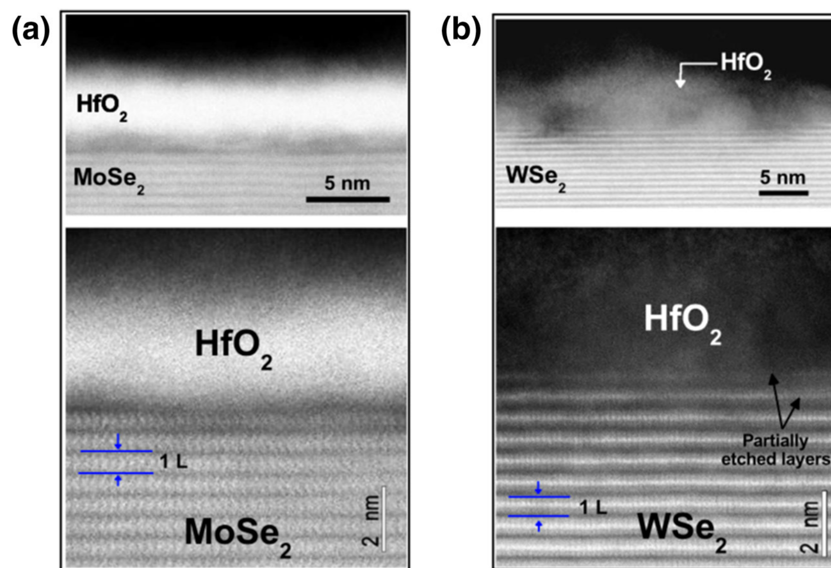

Fig. 12. STEM micrographs corresponding to (a) HfO_2 on UV–O_3 treated $MoSe_2$ and (b) HfO_2 on UV–O_3 treated WSe_2 interfaces. 1L = One layer. Reprinted with permission from Ref. 86.

monolayer properties, which emerge from the bilayer flakes after UV-ozone treatment are due to the screening of the top layer due to the adsorption of oxygen.

Also, UV-O_3 generated by a 4 W Hg lamp in an quartz tube with O_2 flow was used to efficiently oxidize Li-exfoliated MoS_2.[89] In that work, the Li-exfoliated MoS_2 flakes were already partially oxidized prior to UV-O_3 exposure, which suggests that this material is not directly comparable to bulk MoS_2 crystals. Furthermore, the use of flakes provided a large density of edge sites, which are likely to be more prone to oxidation than the basal plane. Similar results showing the Mo oxide after UV-O_3 treatment were reported for solvent exfoliated MoS_2 nanoflakes and MoS_2 quantum dots.[90,91] Park et al. have shown that there may be a source power dependence on the oxidation of exfoliated MoS_2 flakes.[92] These results highlight that the UV-O_3 reaction with MoS_2 is dependent on both the process and the MoS_2 itself. Furthermore, we see evidence of higher reactivity of edge sites that have been shown to oxide even on air exposure.[93] A lower reactivity may be expected for grain boundaries however it has already been shown that mirror twin boundaries in MBE grown $MoSe_2$ acts as favorable nucleation sites for deposited Au.[94] Therefore the details of UV-O_3 reaction with polycrystalline MoS_2 warrant further study.

OTHER FUNCTIONALIZATION STRATEGIES

The UV-O_3 functionalization pretreatment appears to be an ideal solution to nucleating ALD on MoS_2. The deposition requires the use of established UV-O_3 and ALD processes and allows for depositions at moderate temperature of 200°C, which is important for yielding high-quality dielectric films. However, when applied to $MoSe_2$ and WSe_2, it was found that this process was not suitable for functionalization WSe_2 and therefore may not be readily transferable to all TMDCs. It is therefore worthwhile to consider other ozone-based routes to achieving uniform ALD films on TMDCs.

As discussed previously, replacing the H_2O precursor with ozone during and ALD process can impact the uniformity of ALD films on graphene. It was shown that deposition at 200°C yield uniform films.[39] Later work showed that the graphene was highly damage by the ozone, but that uniform films could be achieve by room temperature depositions without damaging the graphene.[43] Similar TMA/O_3 based processes have been explored for both deposition Al_2O_3 on both MoS_2 and WSe_2.[95,96]

When TMA/O_3 deposition on MoS_2 was compared to TMA/H_2O it was found that, at substrate temperatures of 200°C, uniform growth was achieved for the TMA/O_3 process.[95] Atomic force microscopy was used to demonstrate that the films were smooth, while low energy ion scattering spectroscopy was employed to highlight that no Mo or sulfur could be detected, providing evidence that the film was essentially pin-hole free. This result was not unexpected since the same process revealed similar result on graphene,[39] however in the case of MoS_2 it was also shown, via XPS, that there was no evidence of changes to the MoS_2 chemistry (i.e., no oxidation of Mo or S, and no bond scission). Therefore, it appears that a direct TMA/O_3 deposition on MoS_2 at 200°C process can yield uniform films without the need for a functionalization step.

In separate work it was shown that the TMA/O_3 process carried out at 200°C was not readily transferable to WSe_2. Instead, such a process led to reactions with the WSe_2 and non-uniform growth.[96]

The authors investigated the interface chemistry as a function of deposition temperature and found that the reactions could be avoid if the substrate temperature was keep below 150°C, but that uniform deposition was only achieved at room temperature. The authors speculated that this room temperature deposition relied on a non-covalent interaction with the WSe_2 similar to that previously report for graphene.[39,42,97] Room temperature depositions typical yield poor quality films due to the high concentration of partial reaction products left in the film, however by performing a two-step process, the authors were able to deposition Al_2O_3 at 200°C using TMA/O_3 after first seeding the surface with a room temperature deposited layer. This layer had the dual purpose of both seeding the subsequent deposition and also protecting the WSe_2 from reactions with the ozone at 200°C. Electrical device characterization for the 2-step process is under further study.

SUMMARY

The integration of 2D materials into industrial scale device applications will likely require their compatibility with many of the current device fabrication processes. Here, we have focused on ALD, which is a conformal deposition technique that is widely used for the deposition of gate dielectrics. The dearth of dangle bonds on the surface of 2D materials leads to non-conformal deposition that typically forms islands around step edges or defects. A range of functionalization techniques have been explored for the purpose of enabling ALD on 2D materials and many of these have been summarized in this review. For 2D materials beyond MoS_2 it appears that other functionalization process may be superior to UV-O_3 functionalization. For example, low temperature ALD using ozone as the oxidizing precursor can be used to deposit a seed layer for subsequent high temperature deposition. Physical vapor deposited organic or metal seed layers are also commonly reported.

The process of functionalizing the MoS_2 surface with UV-O_3 has been shown to be a robust and facile functionalization technique that has the added benefit of providing a clean (carbon free) and repeatable starting surface. The mechanism appears to involve the rehybridization of the surface sulfur atoms to allow primary bonding to oxygen without any observable S-Mo bond scission. This is confirmed by XPS, and shown to be favorable using density functional theory to model the adsorption. Furthermore, this process has enabled the characterization of top-gated MoS_2 based devices, some of which have shown near ideal subthreshold slopes. While transferring this process to other TMDC materials appears to be non-trivial, it remains to be seen whether control over processing parameters, such as UV power or exposure time could yet result in functionalized TMDCs other than MoS_2.

UV-O_3 treatments have the advantage of utilizing an established industrial surface treatment process. One can envisage the adoption of strategies to monitor functionalized 2D surfaces (and the films grown on them) using a combination of both in-line and out-line characterization tools (e.g., XPS, ellipsometry, Raman, SEM) that are now readily available in the semiconductor industry. However, detailed models need to be created to establish suitable reference sample/spectra correlated to device performance to enable manufacturing control in the semiconductor fabrication environment.

ACKNOWLEDGEMENTS

RMW acknowledges the support of the Erik Jonsson Distinguished Chair at the University of Texas at Dallas.

REFERENCES

1. K. Novoselov, A.K. Geim, S. Morozov, D. Jiang, Y. Zhang, S. Dubonos, I. Grigorieva, and A. Firsov, *Science* 306, 666 (2004).
2. K. Novoselov, D. Jiang, F. Schedin, T. Booth, V. Khotkevich, S. Morozov, and A. Geim, *Proc. Natl. Acad. Sci. USA.* 102, 10451 (2005).
3. T.W. Ebbesen and H. Hiura, *Adv. Mater. (Weinheim, Ger.)* 7, 582 (1995).
4. X. Lu, M. Yu, H. Huang, and R.S. Ruoff, *Nanotechnology* 10, 269 (1999).
5. X.S. Li, W.W. Cai, J.H. An, S. Kim, J. Nah, D.X. Yang, R. Piner, A. Velamakanni, I. Jung, E. Tutuc, S.K. Banerjee, L. Colombo, and R.S. Ruoff, *Science* 324, 1312 (2009).
6. O. Frank and M. Kalbac, *Graphene* (Sawston: Woodhead Publishing, 2014), pp. 27–49.
7. W.A. de Heer, C. Berger, X. Wu, P.N. First, E.H. Conrad, X. Li, T. Li, M. Sprinkle, J. Hass, M.L. Sadowski, M. Potemski, and G. Martinez, *Solid State Commun.* 143, 92 (2007).
8. H. Huang, S. Chen, A.T.S. Wee, and W. Chen, *Graphene* (Sawston: Woodhead Publishing, 2014), pp. 3–26..
9. J.A. Wilson and A.D. Yoffe, *Adv. Phys.* 18, 193–335 (1969).
10. H. Tributsch and J. Bennett, *J. Electroanal. Chem. Interf. Electrochem.* 81, 97 (1977).
11. W. Kautek and H. Gerischer, *Ber. Bunsenges. Phys. Chem.* 84, 645 (1980).
12. W. Kautek, H. Gerischer, and H. Tributsch, *J. Electrochem. Soc.* 127, 2471 (1980).
13. E. Fortin and W. Sears, *J. Phys. Chem. Solids* 43, 881 (1982).
14. H. Boehm, A. Clauss, G. Fischer, and U. Hofmann, *Zeitschrift Für Naturforschung B* 17, 150 (1962).
15. P. Joensen, R. Frindt, and S.R. Morrison, *Mater. Res. Bull.* 21, 457 (1986).
16. B. Radisavljevic, A. Radenovic, J. Brivio, V. Giacometti, and A. Kis, *Nat. Nanotechnol.* 6, 147 (2011).
17. Web of Science citation reports are limited to 10,000 citations, therefore to generate a report for MoS_2 the search had to be refined to include only the following areas. Materials Science Multi-disciplinary, Applied Physics, Nanoscience Nanotechnology, and Electrochemistry.
18. A.K. Geim and I.V. Grigorieva, *Nature* 499, 419 (2013).
19. D.R. Dreyer, R.S. Ruoff, and C.W. Bielawski, *Angew. Chem. Int. Ed.* 49, 9336 (2010).
20. R.S. Ruoff, *MRS Bull.* 37, 1314 (2012).
21. H. Cun, A. Hemmi, E. Miniussi, C. Bernard, B. Probst, K. Liu, D.T. Alexander, A. Kleibert, G. Mette, and M. Weinl, *Nano Lett.* 18, 1205 (2018).
22. T. Greber, arXiv preprint arXiv:0904.1520 (2009).
23. W. Jaegermann and H. Tributsch, *Prog. Surf. Sci.* 29, 1 (1988).

24. S.J. McDonnell and R.M. Wallace, *Thin Solid Films* 616, 482 (2016).
25. S.M. George, *Chem. Rev. (Washington, DC, U. S.)* 110, 111 (2009).
26. H. Kim and W.-J. Maeng, *Thin Solid Films* 517, 2563 (2009).
27. Y. Xuan, Y. Wu, T. Shen, M. Qi, M.A. Capano, J.A. Cooper, and P. Ye, *Appl. Phys. Lett.* 92, 013101 (2008).
28. H.G. Kim and H.-B.-R. Lee, *Chem. Mater.* 29, 3809 (2017).
29. D.B. Farmer and R.G. Gordon, *Nano Lett.* 6, 699 (2006).
30. J. Williams, L. DiCarlo, and C. Marcus, *Science* 317, 638 (2007).
31. R.L. Puurunen, *J. Appl. Phys.* 97, 9 (2005).
32. J.R. Vig and J. LeBus, *IEEE Trans. Parts Hybrids Packag.* 12, 365 (1976).
33. J.R. Vig, *J. Vac. Sci. Technol. A* 3, 1027 (1985).
34. G. Wilk and B. Brar, *IEEE Electron Device Lett.* 20, 132 (1999).
35. Z. Cui, J.M. Madsen, and C.G. Takoudis, *J. Appl. Phys.* 87, 8181 (2000).
36. F. De Smedt, C. Vinckier, I.De Cornelissen, S. Gendt, and M. Heyns, *J. Electrochem. Soc.* 147, 1124 (2000).
37. G. Pant, P. Punchaipetch, M. Kim, R.M. Wallace, and B.E. Gnade, *Thin Solid Films* 460, 242 (2004).
38. P. Punchaipetch, G. Pant, M. Kim, R.M. Wallace, and B.E. Gnade, *J. Vac. Sci. Technolol. A* 22, 395 (2004).
39. B. Lee, S.-Y. Park, H.-C. Kim, K. Cho, E.M. Vogel, M.J. Kim, R.M. Wallace, and J. Kim, *Appl. Phys. Lett.* 92, 203102 (2008).
40. B. Lee, G. Mordi, T. Park, L. Goux, Y.J. Chabal, K. Cho, E.M. Vogel, M. Kim, L. Colombo, and R.M. Wallace, *ECS Trans.* 19, 225 (2009).
41. A. Pirkle, S. McDonnell, B. Lee, J. Kim, L. Colombo, and R.M. Wallace, *Appl. Phys. Lett.* 97, 082901 (2010).
42. S. McDonnell, A. Pirkle, J. Kim, L. Colombo, and R.M. Wallace, *J. Appl. Phys.* 112, 104110 (2012).
43. B. Lee, G. Mordi, M.J. Kim, Y.J. Chabal, E.M. Vogel, R.M. Wallace, K.J. Cho, L. Colombo, and J. Kim, *Appl. Phys. Lett.* 97, 043107 (2010).
44. A.R. Pirkle, Y.J. Chabal, L. Colombo, and R.M. Wallace, *ECS Trans.* 19, 215 (2009).
45. G. Lee, B. Lee, J. Kim, and K. Cho, *J. Phys. Chem. C* 113, 14225 (2009).
46. A. Pirkle, J. Chan, A. Venugopal, D. Hinojos, C.W. Magnuson, S. McDonnell, L. Colombo, E.M. Vogel, R.S. Ruoff, and R.M. Wallace, *Appl. Phys. Lett.* 99, 122108 (2011).
47. J. Chan, A. Venugopal, A. Pirkle, S. McDonnell, D. Hinojos, C.W. Magnuson, R.S. Ruoff, L. Colombo, R.M. Wallace, and E.M. Vogel, *ACS Nano* 6, 3224 (2012).
48. H. Liu and P.D. Ye, *IEEE Electron Device Lett.* 33, 546 (2012).
49. H. Wang, L. Yu, Y.-H. Lee, Y. Shi, A. Hsu, M.L. Chin, L.-J. Li, M. Dubey, J. Kong, and T. Palacios, *Nano Lett.* 12, 4674 (2012).
50. H. Fang, S. Chuang, T.C. Chang, K. Takei, T. Takahashi, and A. Javey, *Nano Lett.* 12, 3788 (2012).
51. H. Liu, K. Xu, X. Zhang, and P.D. Ye, *Appl. Phys. Lett.* 100, 152115 (2012).
52. S. McDonnell, B. Brennan, A. Azcatl, N. Lu, H. Dong, C. Buie, J. Kim, C.L. Hinkle, M.J. Kim, and R.M. Wallace, *ACS Nano* 7, 10354 (2013).
53. A. Azcatl, S. McDonnell, K. Santosh, X. Peng, H. Dong, X. Qin, R. Addou, G.I. Mordi, N. Lu, J. Kim, M.J. Kim, K. Cho, and R.M. Wallace, *Appl. Phys. Lett.* 104, 111601 (2014).
54. R.M. Wallace, *Physics and Technology of High-K Gate Dielectrics 6, ECS Transactions, 214th ECS Meeting*, ed. S. Kar, D. Landheer, M. Houssa, D. Misra, S. Van Elshocht, and H. Iwai, vol. 16, no. 5 (Honolulu, HI, October 12–17, 2008), pp. 255–271.
55. M. Milojevic, F. Aguirre-Tostado, C. Hinkle, H. Kim, E. Vogel, J. Kim, and R. Wallace, *Appl. Phys. Lett.* 93, 202902 (2008).
56. D.M. Hausmann, E. Kim, J. Becker, and R.G. Gordon, *Chem. Mater.* 14, 4350 (2002).
57. S. McDonnell, H. Dong, J.M. Hawkins, B. Brennan, M. Milojevic, F.S. Aguirre-Tostado, D.M. Zhernokletov, C.L. Hinkle, J. Kim, and R.M. Wallace, *Appl. Phys. Lett.* 100, 141606 (2012).
58. Y.-S. Lin, P.-H. Cheng, K.-W. Huang, H.-C. Lin, and M.-J. Chen, *Appl. Surf. Sci.* 443, 421 (2018).
59. X. Zou, J. Xu, H. Huang, Z. Zhu, H. Wang, B. Li, L. Liao, and G. Fang, *Nanotechnology* 29, 245201 (2018).
60. M. Cortez-Valadez, C. Fierro, J. Farias-Mancilla, A. Vargas-Ortiz, M. Flores-Acosta, R. Ramírez-Bon, J. Enriquez-Carrejo, C. Soubervielle-Montalvo, and P. Mani-Gonzalez, *Chem. Phys.* 472, 81 (2016).
61. Y. Hu, H. Jiang, K.M. Lau, and Q. Li, *Semicond. Sci. Technol.* 33, 045004 (2018).
62. T. Roy, M. Tosun, X. Cao, H. Fang, D.-H. Lien, P. Zhao, Y.-Z. Chen, Y.-L. Chueh, J. Guo, and A. Javey, *ACS Nano* 9, 2071 (2015).
63. A. Dahal, R. Addou, A. Azcatl, H. Coy-Diaz, N. Lu, X. de Peng, F. Dios, J. Kim, M.J. Kim, R.M. Wallace, and B. Matthias, *ACS Appl. Mater. Interfaces.* 7, 2082 (2015).
64. B. Fallahazad, S. Kim, L. Colombo, and E. Tutuc, *Appl. Phys. Lett.* 97, 123105 (2010).
65. S. Kim, J. Nah, I. Jo, D. Shahrjerdi, L. Colombo, Z. Yao, E. Tutuc, S.K. Banerjee, arXiv preprint arXiv:0901.2901 (2009).
66. D.B. Farmer, Y.-M. Lin, and P. Avouris, *Appl. Phys. Lett.* 97, 013103 (2010).
67. B. Fallahazad, K. Lee, G. Lian, S. Kim, C.M. Corbet, D.A. Ferrer, L. Colombo, and E. Tutuc, *Appl. Phys. Lett.* 100, 093112 (2012).
68. S. McDonnell, A. Azcatl, G. Mordi, C. Floresca, A. Pirkle, L. Colombo, J. Kim, M. Kim, and R. Wallace, *Appl. Surf. Sci.* 294, 95 (2014).
69. I. McGovern, E. Dietz, H. Rotermund, A. Bradshaw, W. Braun, W. Radlik, and J. McGilp, *Surf. Sci.* 152, 1203 (1985).
70. S. McDonnell, C. Smyth, C.L. Hinkle, and R.M. Wallace, *ACS Appl. Mater. Interf.* 8, 8289 (2016).
71. C.M. Smyth, R. Addou, S. McDonnell, C.L. Hinkle, and R.M. Wallace, *J. Phys. Chem. C* 120, 14719 (2016).
72. C.M. Smyth, R. Addou, S. McDonnell, C.L. Hinkle, and R.M. Wallace, *2D Mater.* 4, 025084 (2017).
73. J.M.P. Alaboson, Q.H. Wang, J.D. Emery, A.L. Lipson, M.J. Bedzyk, J.W. Elam, M.J. Pellin, and M.C. Hersam, *ACS Nano* 5, 5223 (2011).
74. J.H. Park, S. Fathipour, I. Kwak, K. Sardashti, C.F. Ahles, S.F. Wolf, M. Edmonds, S. Vishwanath, H.G. Xing, S.K. Fullerton-Shirey, A. Seabaugh, and A.C. Kummel, *ACS Nano* 10, 6888 (2016).
75. J. Yang, S. Kim, W. Choi, S.H. Park, Y. Jung, M.H. Cho, and H. Kim, *ACS Appl. Mater. Interf.* 5, 4739 (2013).
76. C.L. Hinkle, A.M. Sonnet, E.M. Vogel, S. McDonnell, G.J. Hughes, M. Milojevic, B. Lee, F.S. Aguirre-Tostado, K.J. Choi, J. Kim, and R.M. Wallace, *Appl. Phys. Lett.* 91, 163512 (2007).
77. P. Zhao, P. Vyas, S. McDonnell, P. Bolshakov-Barrett, A. Azcatl, C. Hinkle, P. Hurley, R. Wallace, and C. Young, *Microelectron. Eng.* 147, 151 (2015).
78. H.I. Yang, S. Park, and W. Choi, *Appl. Surf. Sci.* 443, 91 (2018).
79. Q.V. Le, T.P. Nguyen, and S.Y. Kim, *Phys. Status Sol. Rapid Res Lett.* 8, 390 (2014).
80. P. Zhao, A. Azcatl, Y.Y. Gomeniuk, P. Bolshakov, M. Schmidt, S.J. McDonnell, C.L. Hinkle, P.K. Hurley, R.M. Wallace, and C.D. Young, *ACS Appl. Mater. Interf.* 9, 24348 (2017).
81. P. Bolshakov, P. Zhao, A. Azcatl, P.K. Hurley, R.M. Wallace, and C.D. Young, *Appl. Phys. Lett.* 111, 032110 (2017).
82. P. Zhao, A. Azcatl, P. Bolshakov, J. Moon, C.L. Hinkle, P.K. Hurley, R.M. Wallace, and C.D. Young, *J. Vac. Sci. Technol. B* 35, 01A118 (2017).
83. P. Bolshakov, P. Zhao, A. Azcatl, P.K. Hurley, R.M. Wallace, and C.D. Young, *Microelectron. Eng.* 178, 190 (2017).
84. P. Zhao, A. Khosravi, P. Zhao, P.K. Hurley, C.L. Hinkle, R.M. Wallace, and C.D. Young, *2D Mater* 5, 031002 (2018).

85. P. Bolshakov, A. Khosravi, P. Zhao, P.K. Hurley, C.L. Hinkle, R.M. Wallace, and C.D. Young, *Appl. Phys. Lett.* 112, 253502 (2018).
86. A. Azcatl, K. Santosh, X. Peng, N. Lu, S. McDonnell, X. Qin, F. de Dios, R. Addou, J. Kim, M.J. Kim, K. Cho, and R.M. Wallace, *Appl. Phys. Lett.* 112, 253502 (2018).
87. J. Guo, B. Yang, Z. Zheng, and J. Jiang, *Phys. E* 87, 150 (2017).
88. W. Su, N. Kumar, S.J. Spencer, N. Dai, and D. Roy, *Nano. Res.* 8, 3878 (2015).
89. S. Kato, R. Ishikawa, Y. Kubo, H. Shirai, and K. Ueno, *Jpn. J. Appl. Phys.* 50, 071604 (2011).
90. D. Burman, R. Ghosh, S. Santra, S.K. Ray, and P.K. Guha, *Nanotechnology* 28, 435502 (2017).
91. W. Xing, Y. Chen, X. Wang, L. Lv, X. Ouyang, Z. Ge, and H. Huang, *ACS Appl. Mater. Interf.* 8, 26916 (2016).
92. S. Park, S.Y. Kim, Y. Choi, M. Kim, H. Shin, J. Kim, and W. Choi, *ACS Appl. Mater. Interf.* 8, 11189 (2016).
93. R. Addou, C.M. Smyth, J.-Y. Noh, Y.-C. Lin, Y. Pan, S.M. Eichfeld, S. Fölsch, J.A. Robinson, K. Cho, and R.M. Feenstra, *ACS Nano* 11, 5130 (2017).
94. Y. Ma, S.Coy Kolekar, H. Diaz, J. Aprojanz, I. Miccoli, C. Tegenkamp, and M. Batzill, *ACS Nano* 11, 5130 (2017).
95. L. Cheng, X. Qin, A.T. Lucero, A. Azcatl, J. Huang, R.M. Wallace, K. Cho, and J. Kim, *ACS Appl. Mater. Interf.* 6, 11834 (2014).
96. A. Azcatl, Q. Wang, M.J. Kim, and R.M. Wallace, *APL Mater.* 5, 086108 (2017).
97. S. Jandhyala, G. Mordi, B. Lee, G. Lee, C. Floresca, P.-R. Cha, J. Ahn, R.M. Wallace, Y.J. Chabal, and M.J. Kim, *ACS Nano* 6, 2722 (2012).